Duisburg Test Case: Post-Panamax Container Ship for Benchmarking

By Ould el Moctar[1,*], Vladimir Shigunov[2] & Tobias Zorn[2]

ABSTRACT

Duisburg Test Case (DTC) is a hull design of a typical *14000* TEU container ship, developed at the *Institute of Ship Technology, Ocean Engineering and Transport Systems* (ISMT) for benchmarking and validation of numerical methods. Hull geometry and model test results of resistance, propulsion and roll damping are publicly available. The paper presents existing data from model tests and computations.

Key words: Container Ship, Resistance, Seakeeping

1 Introduction

Benchmarking exercises provide a common basis for validation of numerical methods. Several container vessels and corresponding measurement data are publicly available: S175, Kriso Container Ship (KCS) and Hamburg Test Case (HTC). Due to rapid developments in the hull form design of container vessels, there is a need for a typical modern container vessel for benchmarking. *Duisburg Test Case* (DTC) is a hull design of a modern *14000* TEU post-panamax container carrier, developed at the *Institute of Ship Technology, Ocean Engineering and Transport Systems* (ISMT). Although the hull form exists only as a virtual CAD model and as two models in different scales, the lines of the hull represent a typical hull form for modern post-panamax container vessels. This paper describes available data from model tests in scale *1 : 59.407*, conducted in the model test basins *SVA Potsdam* (resistance and propulsion tests), *Nietzschmann* (2010), and *HSVA* (roll decay tests), *Schumacher* (2011). Some computation results are also presented.

2 Geometry and Main Particulars

DTC is a single-screw vessel with a bulbous bow, large bow flare, large stern overhang and a transom. Figure 1 shows hull sections of the vessel; IGES-model is available upon request, *ISMT* (2012).

---

[1] University of Duisburg-Essen, Duisburg, Germany
[2] Germanischer Lloyd SE, Hamburg, Germany
* *Corresponding author*. Present address: ould.el-moctar@uni-due.de

Table 1 shows main particulars in the design loading condition: length between perpendiculars L_{pp}, waterline breadth B_{wl}, draught midships T_m, trim angle ϑ, volume displacement V, block coefficient C_B, wetted surface under rest waterline without appendages S_w and design speed v_d.
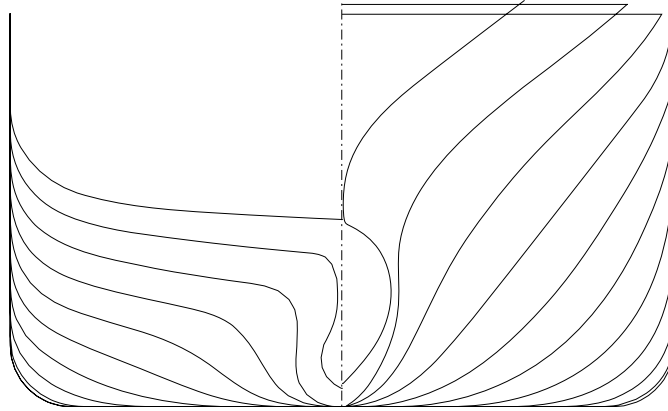

Fig. 1: Hull sections of DTC.

The ship is equipped with a propeller and a rudder, Fig. 2. The propeller is a fixed-pitch five-bladed propeller with right rotation; Table 2 shows its main particulars: propeller diameter D_P, pitch ratio at 0.7 of propeller radius $P_{0.7}/D_P$, disc ratio A_e/A_0, chord length $c_{0.7}$ at 0.7 of propeller radius, effective skew angle of propeller blades θ_{eff} and non-dimensional hub diameter d_h/D_P.

Tab. 1: Main dimensions of DTC in design loading condition.

	Model	Full Scale
L_{pp} [m]	5.976	355.0
B_{wl} [m]	0.859	51.0
T_m [m]	0.244	14.5
ϑ [°]	0.0	0.0
V [m³]	0.827	173467.0
C_B [-]	0.661	0.661
S_w [m²]	6.243	22032.0
v_d [knots]	3.244	25.0

Tab. 2: Propeller parameters.

	Model	Full Scale
D_P [m]	0.150	8.911
$P_{0.7}/D_P$ [-]	0.959	0.959
A_e/A_0 [-]	0.800	0.800
$c_{0.7}$ [mm]	0.054	3.208
θ_{eff} [°]	31.97	31.97
d_h/D_P [-]	0.176	0.176

A twisted rudder equipped with a Costa bulb is used. The base profile is NACA 0018; the rudder is twisted with an angle of $5.0°$ around the shaft axis. The height of the rudder is 12.9 m, measured from the skeg to the baseline. Rudder area is 255.0 m², and the shaft diameter is 1.0 m.

The ship is equipped with a bilge keel, comprised of five segments per ship side. Bilge keel segments are attached in a line following streamlines of the steady flow at design speed and draft. Each segment of the bilge keel has a length of 14.85 m and height of 0.4 m, and a chamfer of length 1.2 m at the forward and aft ends. Segments are located symmetrically with respect to the midship section, separated by gaps of 3.0 m.

3 Resistance and Propulsion Tests

3.1 Loading Conditions

Resistance and propulsion tests were conducted in the model basin *SVA Potsdam* in the design loading condition, Table 1.
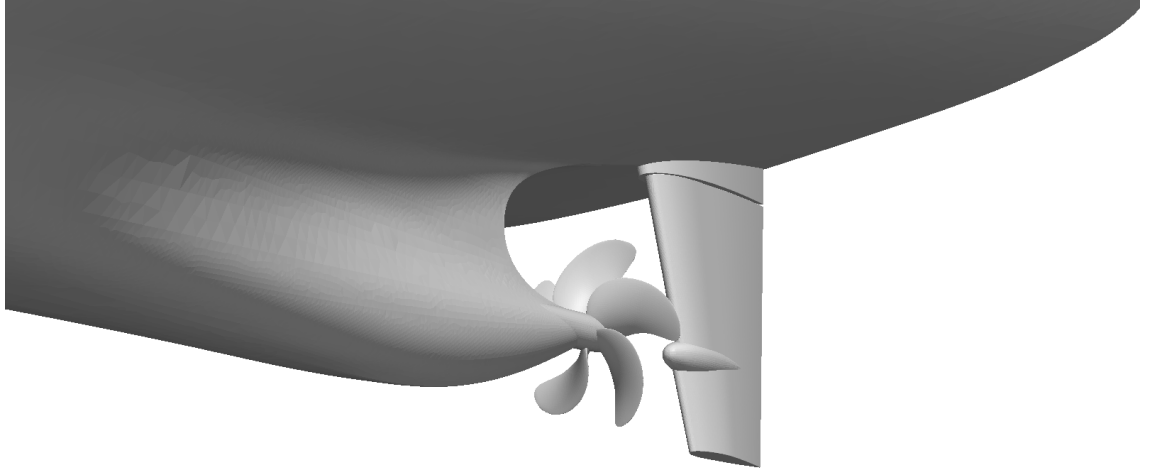
Fig. 2: Ship stern with rudder and propeller.

3.2 Open-Water Propeller Tests

Open-water propeller tests were performed at water kinematic viscosity $1.044 \cdot 10^{-6}$ m^2/s and density 998.47 kg/m^3. Table 3 shows results, including non-dimensional thrust coefficient

$$K_T = T/(\rho D_P^4 n^2) \tag{1}$$

non-dimensional torque coefficient

$$K_Q = Q/(\rho D_P^5 n^2) \tag{2}$$

propeller efficiency

$$\eta_0 = P_T/P_D \tag{3}$$

and thrust loading coefficient

$$C_{Th} = 2T/(\rho v_a^2 A_0) \tag{4}$$

The following definitions are used: T [N] is the propeller thrust, n [1/s] propeller rotation rate, Q [Nm] propeller torque, ρ [kg/m^3] water density, $P_T = T v_a$ [W] thrust power, $P_D = Q\omega$ [W] delivered power, v_a [m/s] propeller advance speed, A_0 [m^2] propeller disc area, $\omega = 2\pi n$ [rad/s] circular frequency of propeller rotation, and $J = v_a/(n D_P)$ propeller advance ratio.

3.3 Resistance Tests

Resistance was measured at six forward speeds, corresponding to Froude numbers $Fr = v/\sqrt{gL_{pp}}$ from 0.172 to 0.214 and full-scale advance speeds v from about 20.0 to 25.0 knots. The hull was ballasted at the design draft 14.5 m with zero trim, and was free in trim and sinkage. Tests were carried out at water kinematic viscosity $\nu_M = 1.090 \cdot 10^{-6}$ m^2/s and density 998.8 kg/m^3.

Table 4 shows results referring to the model scale, including model speed v_m [m/s], Froude number, Reynolds number $Re = \nu_M L_{ppM}/\nu_M$, total resistance R_T [N] and its non-dimensional coefficient $C_T = R_T/(0.5\rho S_w v^2)$, frictional resistance R_F [N] and its non-dimensional coefficient $C_F = R_F/(0.5\rho S_w v^2)$, and non-dimensional wave resistance coefficient $C_W = R_W/(0.5\rho S_w v^2)$.

The frictional resistance coefficient C_F in Table 4 was calculated according to ITTC 1957 as

$$C_F = 0.075/(\log_{10} Re - 2.0)^2 \tag{5}$$

and the wave resistance coefficient was estimated as

$$C_W = C_T - (1 + k)C_F \tag{6}$$

Tab. 3: Results of open-water propeller tests.

J [-]	K_T [-]	$10K_Q$ [-]	η_0 [-]	C_{Th} [-]
0.00	0.509	0.713	0.000	—
0.05	0.492	0.691	0.057	500.7
0.10	0.472	0.667	0.113	120.1
0.15	0.450	0.640	0.168	50.91
0.20	0.427	0.613	0.222	27.17
0.25	0.403	0.584	0.275	16.41
0.30	0.378	0.554	0.326	10.69
0.35	0.353	0.524	0.375	7.333
0.40	0.327	0.493	0.423	5.210
0.45	0.302	0.462	0.468	3.794
0.50	0.276	0.430	0.511	2.812
0.55	0.250	0.398	0.551	2.107
0.60	0.225	0.366	0.586	1.588
0.65	0.199	0.333	0.617	1.196
0.70	0.172	0.299	0.642	0.894
0.75	0.145	0.264	0.657	0.657
0.80	0.118	0.228	0.656	0.467
0.85	0.089	0.191	0.630	0.312
0.90	0.058	0.151	0.553	0.183
0.95	0.026	0.109	0.361	0.074
1.00	−0.009	0.065	−0.209	−0.022

The form factor k was found from a RANSE-CFD simulation for a double-body flow at the model scale as $k = 0.094$ (for reference, RANSE-CFD computed form factor for the full scale is $k = 0.145$).

Tab. 4: Results of resistance model tests.

v_M [m/s]	Fr [-]	$Re \times 10^{-6}$ [-]	R_T [N]	R_F [N]	$C_T \times 10^3$ [-]	$C_F \times 10^3$ [-]	$C_W \times 10^4$ [-]
1.335	0.174	7.319	20.34	17.611	3.661	3.170	1.932
1.401	0.183	7.681	22.06	19.229	3.605	3.142	1.672
1.469	0.192	8.054	24.14	20.964	3.588	3.116	1.791
1.535	0.200	8.415	26.46	22.713	3.602	3.092	2.194
1.602	0.209	8.783	28.99	24.554	3.623	3.069	2.660
1.668	0.218	9.145	31.83	26.431	3.670	3.047	3.360

3.4 Propulsion Tests

Propulsion tests were carried out at the design draught with zero static trim, at the same advance speeds as the resistance tests described above. The model was free in trim and sinkage. Tests were conducted at water temperature $16.8\,°C$, kinematic viscosity of water $\nu_M = 1.090 \cdot 10^{-6}$ m^2/s and water density $\rho_M = 998.8$ kg/m^3.

The British method was used for friction deduction. The model was towed with various forward speeds; for each given forward speed, the propeller rotation rate was varied, and the residual force acting from the carriage on the model (equal to the difference between the propeller thrust and hull resistance including suction force) was measured.

The self-propulsion point of the model, corresponding to the full scale, was found as the rotation rate at which this residual force is equal to the pre-defined difference of two forces: the total model

resistance and the predicted total full-scale resistance, scaled to the model. This difference, called the friction deduction, was calculated in model scale as

$$F_D = 0.5\rho_M S_{wM} v_M^2 (C_{TM} - C_T) \tag{7}$$

where index M denotes model scale. The total resistance coefficient C_T is defined at the corresponding temperature.

The values of the thrust and torque at the full scale self-propulsion point were defined by interpolation over measurement results at the different rotation rates.

With the thus defined thrust T, torque Q and rotation rate n at the self-propulsion point, thrust and torque coefficients are calculated using equations (1) and (2), respectively. Starting with thus defined K_T, the corresponding advance ratio J_T and the torque coefficient K_{QT} are found from the open-water propeller characteristics, Table 3, and then the effective wake fraction with respect to thrust can be calculated as

$$w_T = 1 - J_T D_P / v \tag{8}$$

as well as the relative rotative efficiency

$$\eta_R = K_{QT} / K_Q \tag{9}$$

In a similar way, starting with the K_Q value following from the interpolated torque Q, the corresponding advance ratio J_Q can be found from the open-water propeller characteristics, and the effective wake fraction with respect to torque can be found as

$$w_Q = 1 - J_Q D_P / v \tag{10}$$

In addition to w_T, w_Q and η_R, Table 5 shows thrust deduction fraction t, hull efficiency η_H, propulsive efficiency η_D, propeller efficiency η_0 and the friction deduction F_D [N], calculated using eq. (7).

The thrust deduction fraction is calculated as

$$t = 1 - R_T / T \tag{11}$$

where R_T is the predicted total resistance corresponding to the full scale.

The hull efficiency is defined as

$$\eta_H = P_E / P_T = (1 - t)/(1 - w) \tag{12}$$

where $P_E = Rv$ is the effective power.

The propulsive efficiency is defined as

$$\eta_D = P_E / P_D \tag{13}$$

Tab. 5: Results of propulsion model tests.

v_M [m/s]	t [-]	w_T [-]	w_Q [-]	η_H [-]	η_R [-]	η_D [-]	η_0 [-]	F_{DM} [N]
1.335	0.081	0.264	0.291	1.249	0.959	0.720	0.602	9.419
1.401	0.101	0.279	0.293	1.247	0.980	0.729	0.596	10.256
1.469	0.093	0.277	0.291	1.255	0.978	0.734	0.598	11.146
1.535	0.089	0.281	0.294	1.266	0.979	0.739	0.596	12.047
1.602	0.101	0.277	0.284	1.245	0.989	0.730	0.593	12.985
1.668	0.090	0.275	0.279	1.255	0.993	0.738	0.592	13.947

4 Roll Damping Tests

4.1 Loading Conditions

Roll decay tests were carried out at *HSVA* with the same model. Two loading conditions were realised, corresponding to the full-scale draughts of *12.0* and *14.0* m. Table 6 shows main parameters, including, in addition to those parameters shown in Table 1, the height KM_t of the transverse metacentre above the keel, transverse metacentric height GM_t, height KG of the centre of gravity above the keel, natural period of small roll oscillations T_φ, and dry longitudinal k_{xx}, transversal k_{yy} and vertical k_{zz} radii of inertia with respect to the centre of gravity.

Tab. 6: Loading conditions realised in roll damping measurements (numbers are given in the full scale).

T_m [m]	12.0	14.0
ϑ [°]	0.0	0.0
V [m³]	136617.5	165868.5
C_B [-]	0.6288	0.6544
KM_t [m]	25.95	25.05
GM_t [m]	4.57	1.37
KG [m]	21.38	23.68
T_φ [s]	20.36	38.17
k_{xx} [m]	19.39	20.25
k_{yy} [m]	95.86	88.19
k_{zz} [m]	95.80	88.49

4.2 Roll Damping Measurements according to *Blume* (1979)

Blume (1979) method of defining effective linear damping is based on the application of a time-harmonic exciting roll moment of known frequency and amplitude. The model is free in all degrees of freedom, and the roll amplitude of stationary oscillations is measured. The excitation roll moment is imposed by two masses, rotating with same frequency in opposite direction around a vertical axis; the masses meet twice per rotation period at the farthest points from the central plane.

The excitation frequency is systematically varied in small steps near the resonance to find the resonance frequency ω_φ and the corresponding resonance roll amplitude φ_{res}. Because both the natural roll frequency and the effective linear roll damping depend on the roll amplitude, the tests are repeated for systematically varied amplitudes of the excitation moment. The results are presented as effective linear roll roll damping vs. resonance roll amplitude at the resonance frequency.

A static moment M results in a heel angle $\varphi_{stat} = M/c_\varphi$, where $c_\varphi = mgGM_t$ is the stiffness coefficient and m is the mass displacement. Applying a harmonically oscillating moment $M \sin \omega_\varphi t$ with the same amplitude M at the resonance frequency $\omega_\varphi = \sqrt{c_\varphi/I_\varphi}$, where I_φ is the moment of inertia with respect to the roll axis (including added moment of inertia), can be described by a linearised uncoupled roll equation

$$I_\varphi \ddot{\varphi} + b_{eff} \dot{\varphi} + c_\varphi \varphi = M \sin \omega_\varphi t \tag{14}$$

where b_{eff} is the coefficient of the equivalent linear roll damping, and φ is the roll angle.

Note that if the same masses are used to impose both the static heeling moment M and the harmonically oscillating moment, the amplitude of the harmonically oscillating excitation moment will differ from M due to the centrifugal force. In experiments, the results are corrected for this effect; here the results are presented in such a way that the static heeling moment and the amplitude of the harmonic excitation moment in eq. (14) can be assumed equal.

The resonance roll amplitude corresponding to eq. (14) is

$$\varphi_{res} = \frac{M}{b_{eff}} \sqrt{\frac{I_\varphi}{c_\varphi}} \tag{15}$$

and therefore

$$\varphi_{stat}/\varphi_{res} = b_{eff} / \sqrt{I_\varphi c_\varphi} \tag{16}$$

or

$$b_{eff} = \frac{\varphi_{stat}}{\varphi_{res}} \frac{c_\varphi}{\omega_\varphi} \tag{17}$$

thus the ratio $\varphi_{stat}/\varphi_{res}$ can also be used to describe the effective linear damping coefficient.

Roll damping was measured at three forward speeds of the model, *0.0, 0.8* and *1.47* m/s, corresponding to the full-scale speeds of *0.0, 12.0* and *22.0* knots, respectively. The model was self-propelled using automatically controlled propeller. Because roll motion changes the resistance of the model, the required forward speed was not exactly matched. Tables 7 and 8 show results of excited roll tests for the two loading conditions with the full-scale draught *12.0* and *14.0* m, respectively, including forward speed *v* (given in full scale), resonance roll amplitude φ_{res}, resonance roll frequency ω_φ (given in full scale) and the non-dimensional effective linear damping coefficient $\varphi_{stat}/\varphi_{res}$.

Tab. 7: Results of excited roll test at the full-scale draught of *12.0* m.

v [knots]	φ_{res} [°]	ω_φ [rad/s]	$\varphi_{stat}/\varphi_{res}$ [-]
0.0	*7.40*	*0.308*	*0.036*
0.0	*8.98*	*0.310*	*0.041*
0.0	*12.80*	*0.311*	*0.064*
0.0	*19.15*	*0.314*	*0.127*
11.9	*4.88*	*0.307*	*0.055*
12.2	*10.81*	*0.310*	*0.094*
11.9	*16.67*	*0.316*	*0.146*
22.9	*5.45*	*0.320*	*0.149*
21.9	*12.89*	*0.323*	*0.188*
20.9	*20.68*	*0.327*	*0.244*

Tab. 8: Results of excited roll test at the full-scale draught of *14.0* m.

v [knots]	φ_{res} [°]	ω_φ [rad/s]	$\varphi_{stat}/\varphi_{res}$ [-]
0.0	*5.78*	*0.164*	*0.040*
0.0	*10.04*	*0.168*	*0.046*
0.0	*17.46*	*0.178*	*0.083*
11.9	*4.97*	*0.169*	*0.094*
12.2	*11.47*	*0.176*	*0.127*
11.9	*17.17*	*0.182*	*0.173*
22.7	*5.05*	*0.183*	*0.287*
22.5	*9.99*	*0.183*	*0.298*
21.3	*18.71*	*0.191*	*0.361*

Note that Tables 7 and 8 show effective linear roll damping for those roll amplitudes that were realised in the experiments. In numerical simulations, roll damping coefficients are usually required at some prescribed roll amplitudes. Therefore, the dependency of the effective linear roll damping on roll amplitude in Tables 7 and 8 was plotted and re-evaluated at the roll amplitudes of *5.0, 10.0, 15.0* and *20.0°*, Table 9.

4.3 Roll Decay Tests

In a free roll decay test, the model is heeled in calm water to an initial heel angle and released; the model starts to perform free decaying oscillations with frequency depending on the amplitude. Roll decay tests were carried out in the same two loading conditions, corresponding to the full-scale draughts of *12.0* and *14.0* m, Table 6, with a free-sailing self-propelled model at three forward speeds $v_M = $ *0.0, 0.8* and *1.479* m/s. In zero forward-speed tests, roll motion was excited by an initial disturbance. In the tests with a non-zero forward speed, the model was first heeled to a heel angle of about *16* to *20°* using a weight, placed on the model unsymmetrically with respect to the central plane. The model then accelerated in the heeled state due to propeller to required forward speed. The yaw moment, acting on the model due to the unsymmetrical submerged part, was compensated by the rudder, steered with an autopilot. After achieving the required forward speed, the weight

Tab. 9: Coefficients $\varphi_{stat}/\varphi_{res}$ of equivalent linear roll damping vs. roll amplitude and forward speed.

φ_{res} [°]	$T_m =$	12.0 m	$T_m =$	14.0 m
	Fr [-]	$\varphi_{stat}/\varphi_{res}$ [-]	Fr [-]	$\varphi_{stat}/\varphi_{res}$ [-]
5.0	0.000	0.030	0.000	0.039
5.0	0.104	0.055	0.104	0.094
5.0	0.200	0.147	0.198	0.198
10.0	0.000	0.046	0.000	0.047
10.0	0.106	0.088	0.106	0.117
10.0	0.194	0.171	0.196	0.299
15.0	0.000	0.081	0.000	0.068
15.0	0.105	0.130	0.105	0.154
15.0	0.189	0.202	0.191	0.329
20.0	0.000	0.137	0.000	0.101
20.0	0.101	0.181	0.104	0.203
20.0	0.183	0.238	0.183	0.374

was removed using a rope system, attached to the carriage, following the model, and the model started free decaying oscillations. Yaw oscillations, excited due to yaw coupling with roll motion, were controlled with the rudder, and the forward speed was adjusted by controlling the propeller rotation rate. Both the rudder and propeller were steered with an autopilot.

Figures 3 and 4 show measured roll decay time histories for the loading conditions with the full-scale draughts *12.0* and *14.0* m, respectively.

For a homogeneous linearised decoupled roll equation

$$I_\varphi \ddot{\varphi} + b_{eff} \dot{\varphi} + c_\varphi \varphi = 0 \tag{18}$$

with non-zero initial conditions, oscillatory solutions exist if the effective linear roll damping coefficient b_{eff} is less than the critical roll damping $b_{cr} = 2\sqrt{I_\varphi c_\varphi}$. For ships, $b_{eff} \ll b_{cr}$, and the solution is a decaying oscillation, for which the influence of damping on the natural roll frequency ω_φ can be neglected, thus $\omega_\varphi = \sqrt{c_\varphi/I_\varphi}$.

Different quantities can be used to describe roll decay, for example, roll decrement of nth order, defined as

$$\Delta_n = \varphi_{a,i}/\varphi_{a,i+n} \tag{19}$$

i.e. the ratio of roll amplitudes φ_a separated by n roll periods. Most often, the first-order decrement Δ_1 (or simply Δ) is used, $\Delta = \varphi_{a,i}/\varphi_{a,i+1}$; from the solution of eq. (18),

$$\Delta = \exp\left[\pi b_{eff}/(\omega_\varphi I_\varphi)\right] \tag{20}$$

Natural logarithm of the first-order decrement $\ln \Delta$, called logarithmic decrement, is also frequently used. Note that according to eq. (20),

$$\delta \equiv \ln \Delta = \pi b_{eff}/(\omega_\varphi I_\varphi) \tag{21}$$

Another frequently used measure is the ratio of the effective linear roll damping coefficient b_{eff} to the critical damping b_{cr},

$$\zeta \equiv b_{eff}/b_{cr} = \delta/(2\pi) \tag{22}$$

often expressed as percentage. Remembering eq. (17), we can relate roll damping characteristics from forced roll and free roll decay tests as

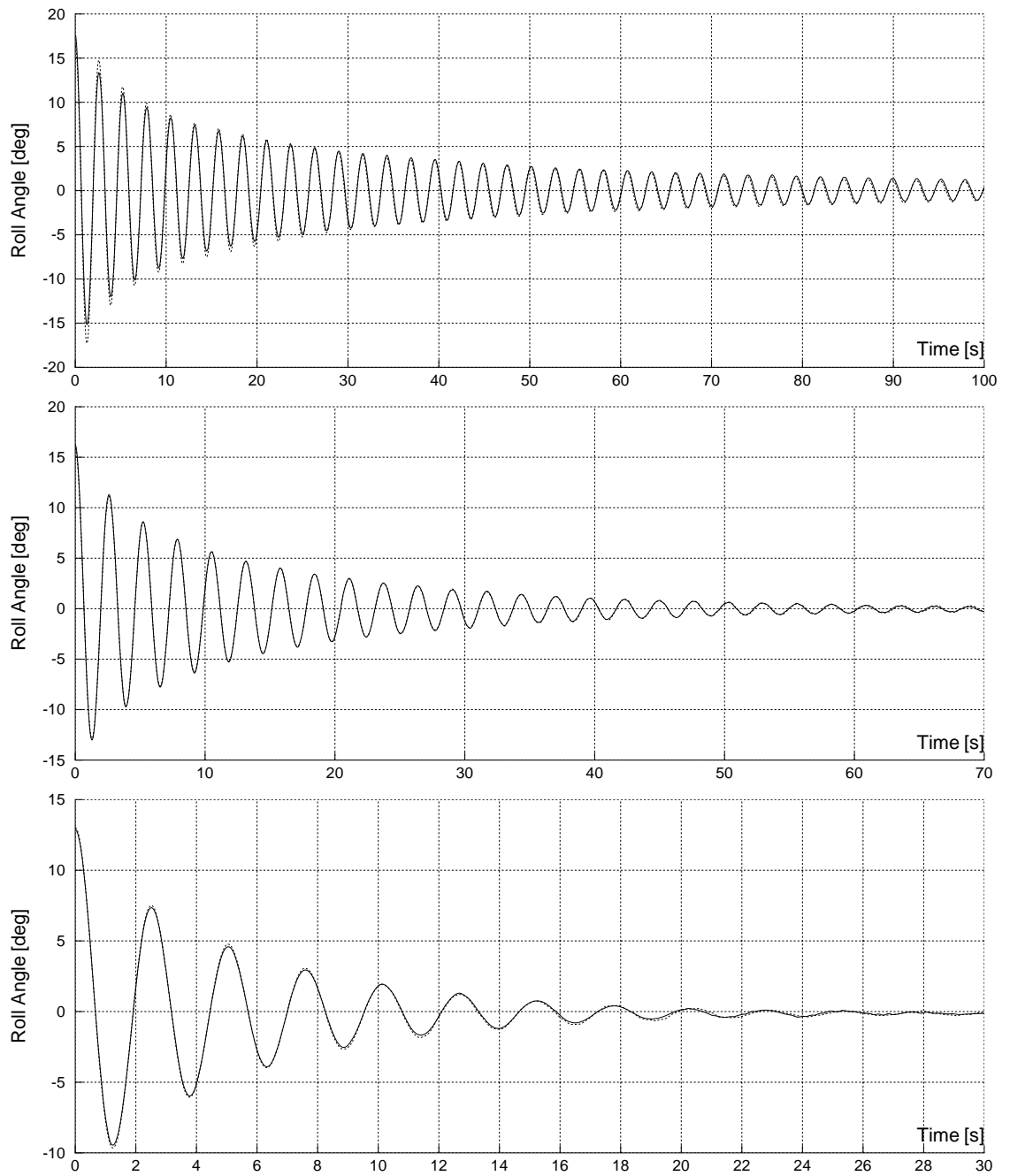$$\zeta = \delta/(2\pi) = 0.5\varphi_{stat}/\varphi_{res} = 0.5 b_{eff}/\sqrt{I_\varphi c_\varphi} \tag{23}$$

Fig. 3: Measured roll angle time histories for the full-scale draught of *12.0* m at the model forward speed of *0.0* (top), *0.8* (middle) and *1.47* (bottom) m/s. Multiple time histories on the same plot correspond to repeated tests.
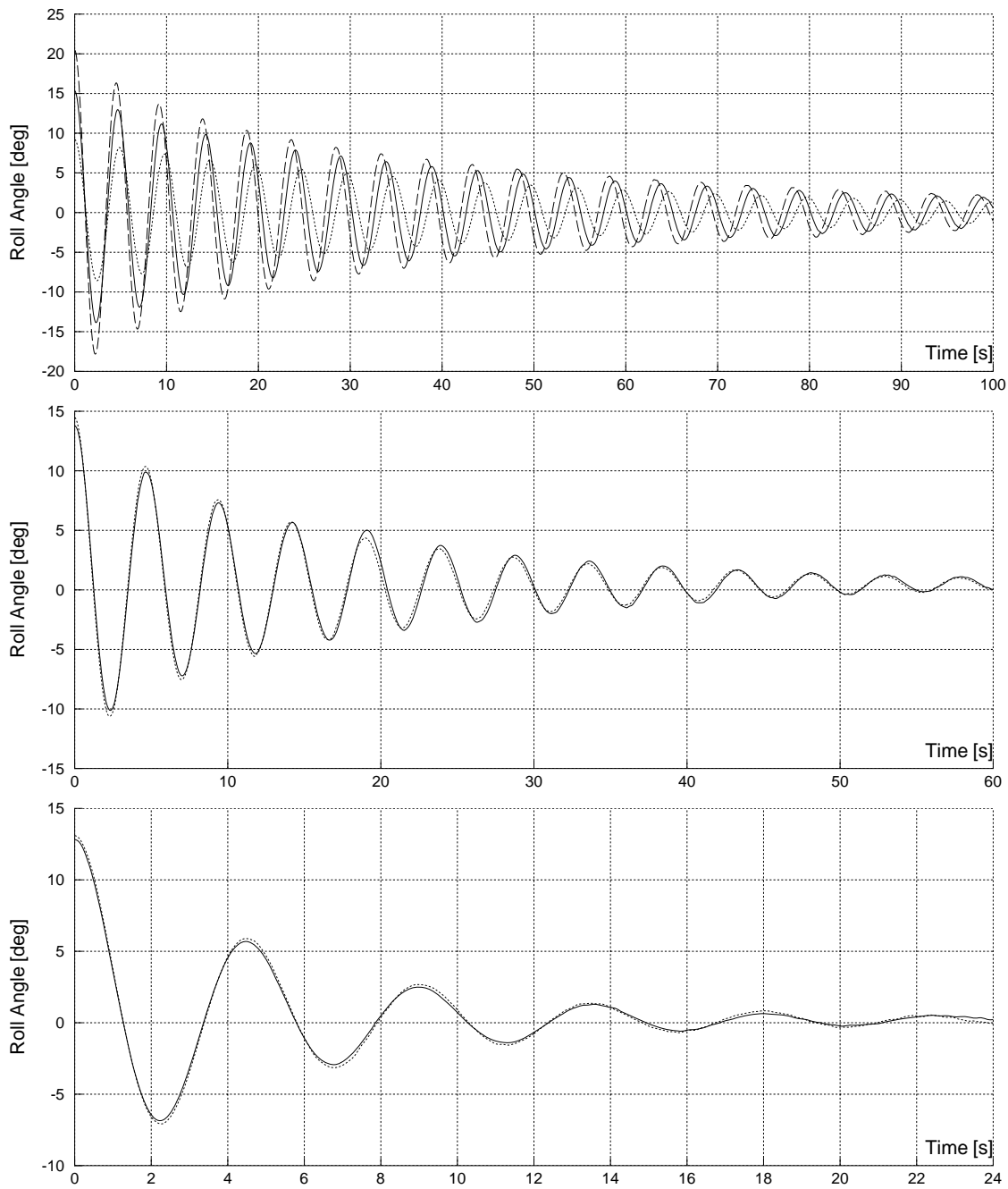
Fig. 4: Measured roll angle time histories for the full-scale draught of *14.0* m at the model forward speed of *0.0* (top), *0.8* (middle) and *1.47* (bottom) m/s. Multiple time histories on the same plot correspond to repeated tests.

The following method was used to find the decrement of decaying roll oscillations, Fig. 5: first, find all positive $\varphi_{a+}^{(i)}$ and all negative $\varphi_{a-}^{(i)}$ roll amplitudes; $\varphi_{a-}^{(i)}$ is defined here as the negative roll amplitude half-period after the positive amplitude $\varphi_{a+}^{(i)}$. Logarithmic decrement is plotted as points $\ln[\varphi_{a+}^{(i)}/\varphi_{a+}^{(i+1)}]$ and $\ln[\varphi_{a-}^{(i)}/\varphi_{a-}^{(i+1)}]$ (vertical axis) vs. $\varphi_{a-}^{(i)}$ and $\varphi_{a+}^{(i+1)}$ (horizontal axis), respectively. A linear or quadratic fit to the dependency $\delta(\varphi_a)$ produces, respectively, quadratic or cubic dependency of the equivalent linear roll damping coefficient b_{eff} on the roll amplitude. Note that, according to eq. (21), also the natural frequency is required at the actual roll amplitude to find b_{eff} from δ. The dependency $\omega_\varphi(\varphi_a)$ is also found by post-processing of the roll decay test, Fig. 6; this time, the time intervals between $\varphi_{a+}^{(i)}$ and $\varphi_{a+}^{(i+1)}$ are plotted vs. $\varphi_{a-}^{(i)}$, and the time intervals between $\varphi_{a-}^{(i)}$ and $\varphi_{a-}^{(i+1)}$ are plotted vs. $\varphi_{a+}^{(i+1)}$ on the same plot.

Figures 7 and 8 show equivalent linear roll damping (expressed as a fraction of the critical damping) vs. roll amplitude for the loading conditions with the full-scale draughts 12.0 and 14.0 m, respectively, for all forward speeds.
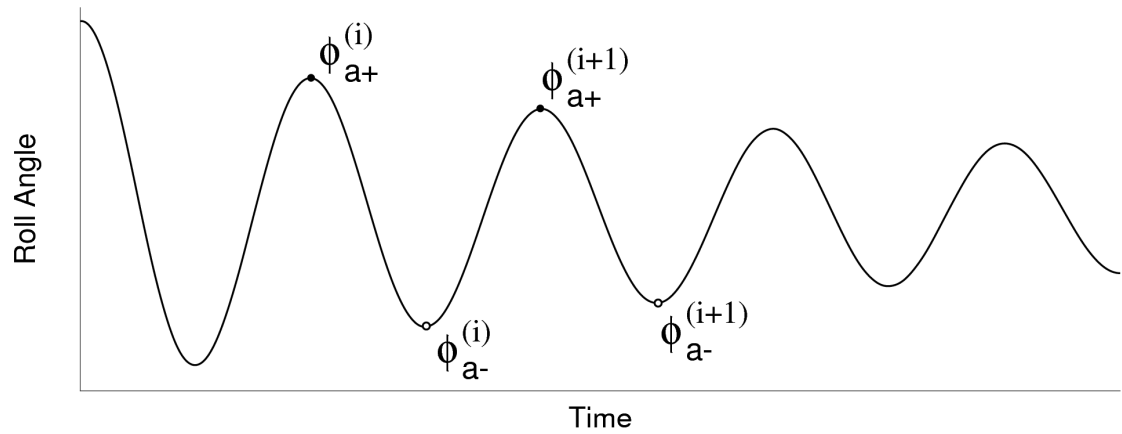

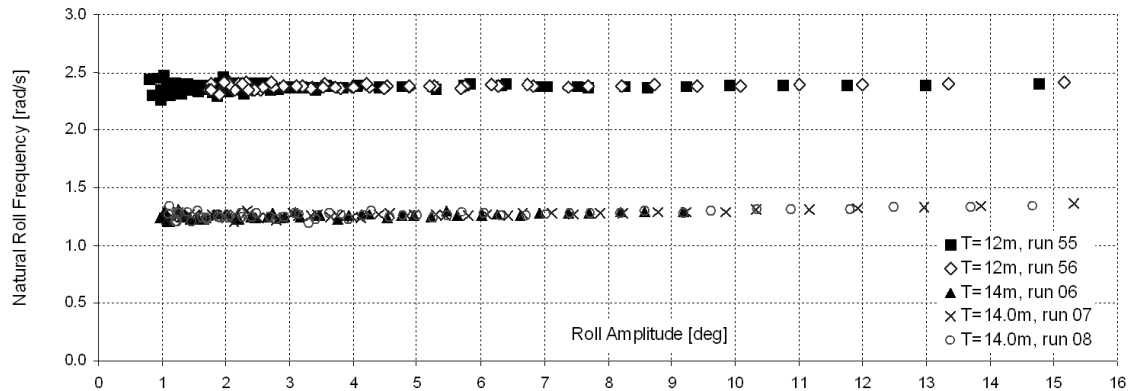Fig. 5: Post-processing of roll decay test.

Fig. 6: Natural roll frequency ω_φ [rad/s] vs. roll amplitude φ_a [°] from roll decay tests for loading conditions with the full-scale draught of 12.0 and 14.0 m at zero forward speed. Multiple symbols for the same loading condition correspond to repeated tests.
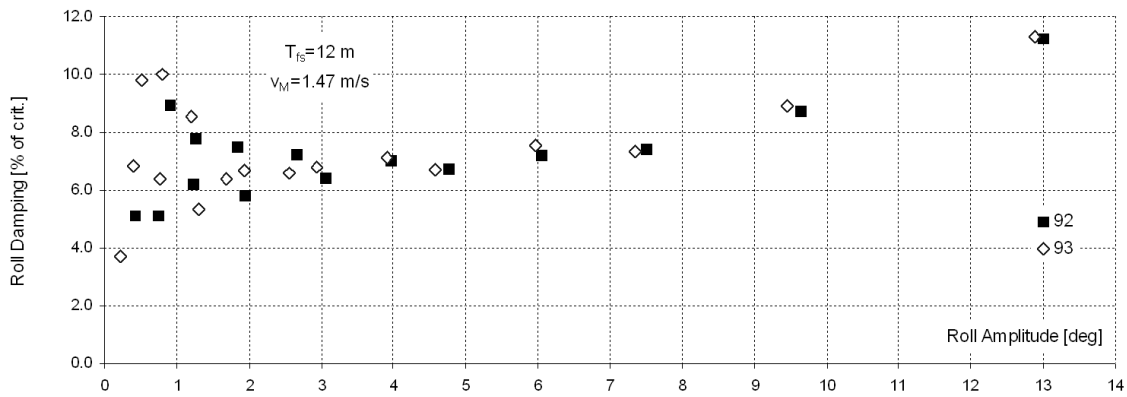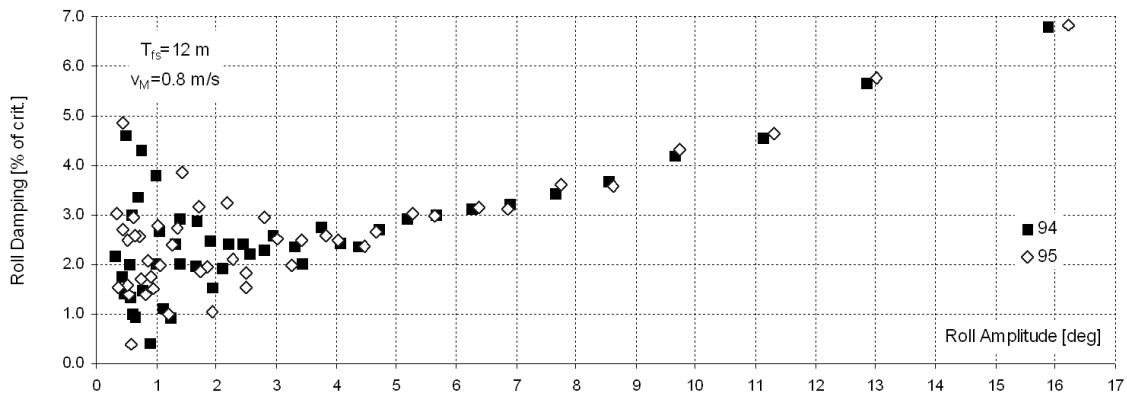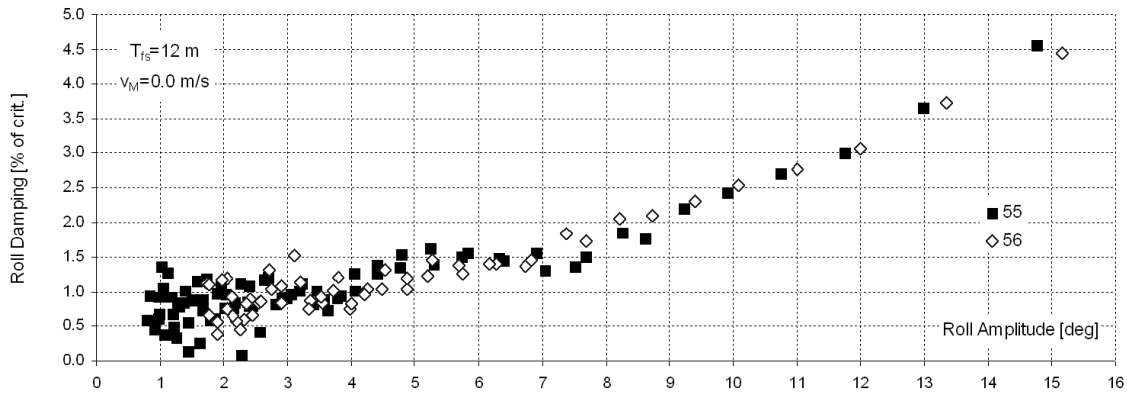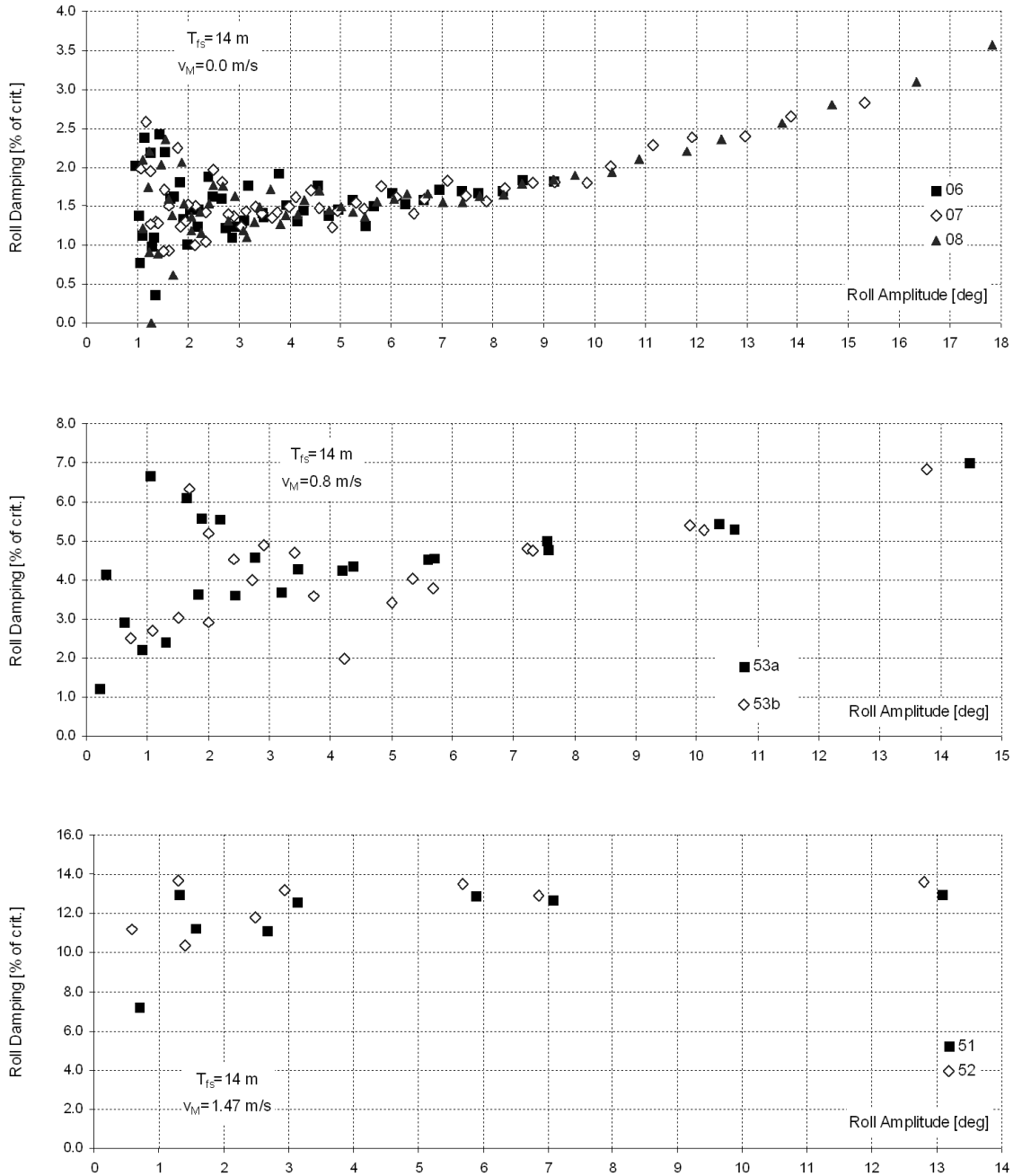
60

Fig. 7: Equivalent linear roll damping as percentage of critical damping from model tests for loading condition with the full-scale draught of *12.0* m at model forward speeds of *0.0* (top), *0.8* (middle) and *1.47* (bottom) m/s. Different symbols on one plot correspond to repeated tests.

Fig. 8: Equivalent linear roll damping as percentage of critical damping from model tests for loading condition with the full-scale draught of *14.0* m at model forward speeds of *0.0* (top), *0.8* (middle) and *1.47* (bottom) m/s. Different symbols on the same plot correspond to repeated runs.

5 Examples of Numerical Results

5.1 Resistance

Figure 9 shows the total resistance (left) and the estimated wave-making part of the resistance (right) of the model, computed with a RANSE-CFD code, in comparison with measurements. In RANSE-CFD computations, shear stresses and pressures were integrated separately, to provide friction R_F and pressure R_P contributions to the total resistance, respectively. The pressure contribution contains wave-making component R_W and the viscous pressure resistance R_{VP}. In order to find the latter contribution, it was assumed proportional to the friction resistance,

$$R_{VP} = kR_F \tag{24}$$

where k is the form-factor. To find the form-factor, RANSE-CFD computations for a double-body flow were carried out, and the form-factor k was found from

$$1 + k = R_T^{db}/R_F^{db} \tag{25}$$

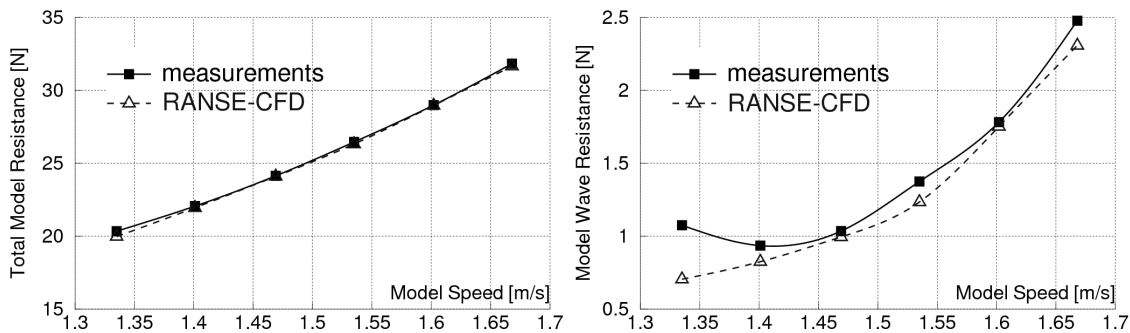(index db denotes double-body flow).

Fig. 9: Total (left) and wave–making (right) resistance of the model from measurements (solid line) and RANSE–CFD computations (dashed line) vs. model speed.

Using this form-factor, the wave-making part of the resistance was calculated for model test and RANSE-CFD results as

$$R_W = R_T - (1 + k)R_F \tag{26}$$

where friction resistance R_F was taken from RANSE-CFD simulations with the free surface.

5.2 Roll Decay

Figure 10 shows roll decay measurement and RANSE-CFD simulation for the loading condition with full-scale draught *12.0* m at zero forward speed, and Figure 11 shows roll decay measurement and RANSE-CFD simulation for the loading condition with full-scale draught *14.0* m at the maximum forward speed (*1.47* m/s). Roll motion in RANSE-CFD simulations corresponds well with the measurements for the case without forward speed; in the simulations with forward speed, measurements show significantly larger roll damping.

Because the differences between the simulations and measurements increase with the increasing forward speed, the reason was assumed to be the lift component of the roll damping due to the differences in the lift forces on the hull and appendages. To study the reasons for the differences, the simulation for the full-scale draught *14.0* m with the model forward speed of *1.47* m/s was repeated with different model settings including simulations with free yaw motion and a controlled rudder.

The simulation with free yaw shows increase in roll damping, because free yaw increases relative motion between the hull and water, especially at the bow, which contributes to the lift component of roll damping. In the simulation with free yaw and controlled rudder, the rudder was

geometrically modelled and able to move. To simulate rudder forces accurately, propeller race was also modelled by longitudinal momentum sources, distributed in the propeller disc. The steering of the rudder angle was done according to the rudder angle time history from the model test. This simulation shows significantly larger roll damping than in the simulation without rudder and with restrained yaw.

This study shows that lift forces on the hull and especially on the rudder can produce a significant contribution to roll damping with forward speed. The remaining differences between the simulations and model tests require further study.
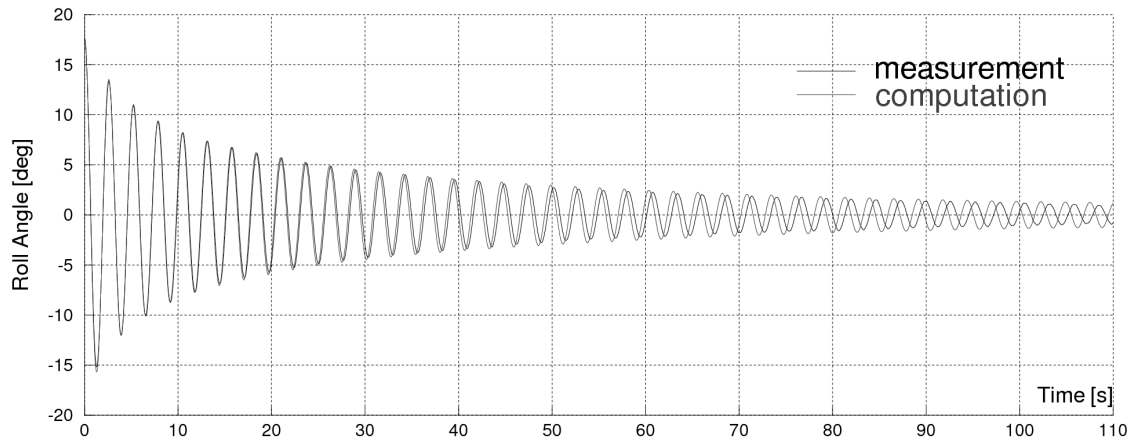

Fig. 10: Roll decay measurement and RANSE-CFD simulation for the loading condition with full-scale draught *12.0* m at zero forward speed.
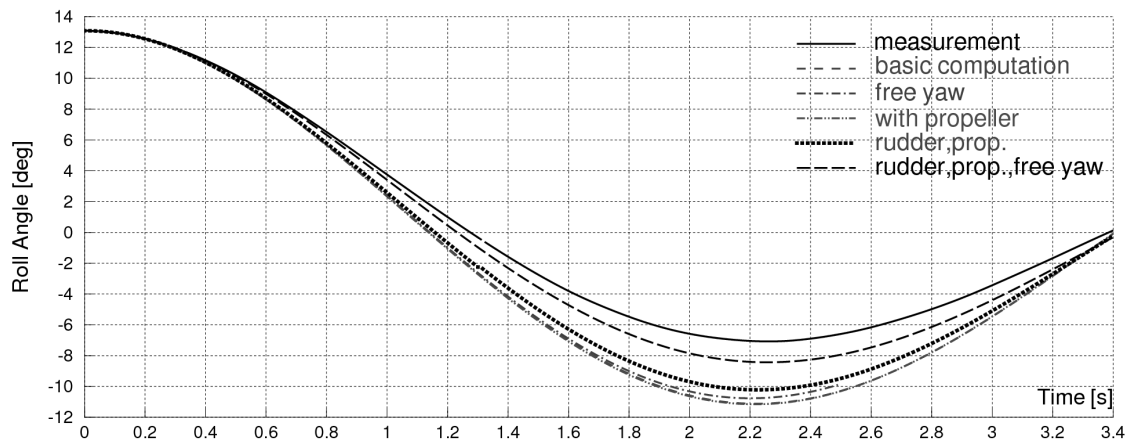

Fig. 11: Roll decay measurement and RANSE-CFD simulation for the loading condition with full-scale draught *14.0* m at the maximum model forward speed (*1.47* m/s).

References

Blume, P. *(1979).* Experimentelle Bestimmung von Koeffizienten der wirksamen Rolldämpfung und ihre Anwendung zu Abschätzung extremer Rollwinkel. *Schiffstechnik, 26*

ISMT *(2012).* `http://www.uni-due.de/ISMT/`. *Institute of Ship Technology, Ocean Engineering Project BestRollTransport Systems, University Duisburg-Essen*

Nietzschmann, T. *(2010).* Widerstands- und Propulsionsversuch für das Modell eines Containerschiffes. *SVA Potsdam Model Basin*

Schumacher, A. *(2011).* Rolldämpfungsversuche mit dem Modell eines groß en Containerschiffes. *The Hamburg Ship Model Basin*